

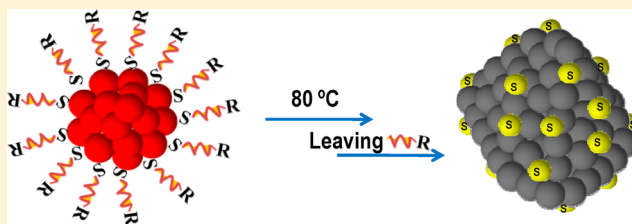
Low-Temperature Thermal Dissociation of Ag Quantum Clusters in Solution and Formation of Monodisperse Ag₂S Nanoparticles

Kadamkotte Puthenveetil Remya, Thumu Udayabhaskararao, and Thalappil Pradeep*

DST Unit of Nanoscience (DST UNS), Indian Institute of Technology, Madras, Chennai 600 036, India

S Supporting Information

ABSTRACT: We report the effect of temperature on the stability of glutathione-protected Ag₂₅ clusters. The clusters are stable up to 50 °C. Interestingly, above this temperature, they decompose to yield Ag₂S nanoparticles with an average diameter of 3 ± 1 nm, crystallizing in monoclinic acanthite polymorph. Unlike conventional methods of syntheses of Ag₂S, where a temperature of ~200 °C is needed, our study shows the possibility of synthesis of Ag₂S nanoparticles at much lower temperatures. This is in contrast with silver nanoparticles protected with thiolates, which typically give silver and alkyl/aryl disulfide upon thermal activation. The mechanism of cluster decomposition and formation of silver sulphide nanoparticles was investigated using various analytical techniques such as ultraviolet–visible spectroscopy, X-ray diffraction scanning electron microscopy, energy-dispersive analysis of X-rays, transmission electron microscopy, and electrospray ionization mass spectrometry. The monolayer of the cluster undergoes S–C bond cleavage, as revealed by mass spectrometry. This is somewhat unusual because Ag–S cleavage is expected in view of its lower bond energy.



1. INTRODUCTION

Noble-metal nanoparticles with thiolate protection^{1–4} have been extensively investigated in the past several years because of their interesting electrical, optical, and chemical properties and due to their possible applications in various fields. Their properties are highly influenced by the medium, nature of the protecting ligand, pH, temperature, and so on, of which temperature is of high importance. Thermal stability of such monolayer-protected nanoparticles, referred to as MPCs (monolayer-protected clusters), previously has been a subject of discussion.⁵ Thermal desorption of MPCs of gold results in the formation of alkyl disulfide in the gas phase and gold in the solid state, the Au–S bond being stable till 160 °C. Similar decomposition takes place in the case of silver as well.^{6–8} For example, carboxylates of silver decompose to give metallic silver and carboxylic acid derivatives or radicals upon heating.⁹ Thermal desorption of thiolate self-assembled monolayers (SAMs) on planar surfaces can also distinguish adsorption sites.^{10,5b}

Noble-metal-derived quantum clusters¹³ are exciting new materials. They exhibit unique properties due to the confinement of electrons in discrete energy levels. These subnanometer particles having a core of only a few metal atoms can be considered as the smallest analogues of MPCs. Bare cores are inherently unstable because of their high surface energy, which makes them coalesce into larger particles. Such cores could be protected and stabilized with a shell of ligands, and the system as a whole exhibits interesting optical and chemical properties. The ligand shell plays an important role in determining the properties of clusters such as their stability as well as physical and chemical properties.^{2,14,15} Study of these properties has attracted significant attention in the recent past. Study of applications of nanoclusters has been a subject of interest as well.

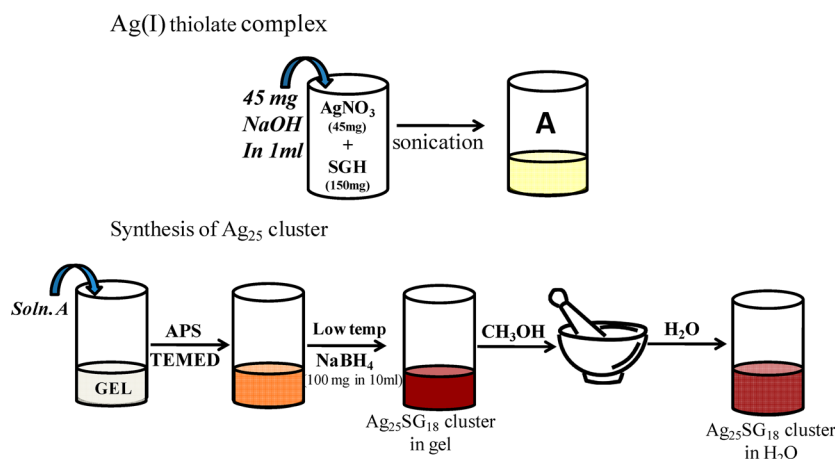
Most of the studies in this category of materials have been on gold clusters, especially Au₂₅SG₁₈. (SG is glutathione in the thiolate form, protecting the Au₂₅ core.) Silver clusters are the second most studied systems. These clusters exhibit bright fluorescence with a quantum yield up to 64%.¹⁶ Practical applications of clusters are determined by their stability under ambient conditions.¹⁷ The stability increases upon going from free to supported to passivated clusters.¹⁸ Some of the new areas of research of these materials are: (i) incorporating them in human cells¹⁹ as a diagnostic tool,^{20,21} (ii) fabrication of luminescent patterns,²² (iii) catalysis,^{23–25} (iv) metal ions sensing,^{26–28} (v) biolabeling,²⁹ and (vi) medicine.³⁰

Most of these applications would require an understanding of the thermal stability of the material of interest. We report the experimental results of our study of thermal stability of QCs, taking Ag₂₅SG₁₈ as a model. We find that these clusters undergo thiolate desorption and heterolytic bond cleavages, resulting in the formation of Ag₂S nanoparticles at low temperatures. Mechanistic aspects of the reaction were probed with several spectroscopic tools. The only related studies have been on the temperature-dependent optical properties of Au₂₅SR₁₈ in solution,¹¹ but the product of dissociation was not further investigated. It is likely to be Au(I)-thiolates. However, because the chemistry of gold clusters is quite different from that of silver, the products of thermal decomposition may vary for silver clusters. One such example is the heating of aryl-thiolated silver nanoparticles having non-plasmonic optical properties at 90 °C, leading to the formation of

Received: July 7, 2012

Revised: October 28, 2012

Published: November 7, 2012

Scheme 1. Synthetic Procedure Used to Make $\text{Ag}_{25}\text{SG}_{18}$ Clusters

nanoparticles, which show single plasmon-like resonance in their optical spectrum.¹²

Ag_2S is a direct band gap semiconductor with a narrow band gap. Its excellent optical-limiting properties and high stability, especially in nanoparticle form, enable potential applications in the field of microelectronics, IR detectors, memory devices (Giant Magneto Resistance), and so on. In general, the synthesis of Ag_2S nanoparticles requires high temperature and complex processes. Only a few reports exist on the preparation based on emulsion methods. We emphasize that our low-temperature route for the synthesis of Ag_2S nanoparticles may be explored as a general synthetic method that may be useful for preparations starting with other quantum clusters and diverse ligands.

2. EXPERIMENTAL SECTION

2.1. Materials. Silver nitrate (99%), glutathione (GSH, 97%), methanol (GR grade), acrylamide (AR grade), N,N' -methylenebisacrylamide (BIS, AR grade), ammonium persulfate, and N,N,N',N' -tetramethylethylenediamine (TEMED) were purchased from SRL Chemical, India. Other chemicals used are: (1) sodium borohydride (NaBH_4 , 99.99%, Aldrich) and (2) ethanol, methanol, and dichloromethane (all HPLC grade, Aldrich). All chemicals were used without further purification.

2.2. Synthesis of $\text{Ag}_{25}\text{SG}_{18}$. $\text{Ag}_{25}\text{SG}_{18}$ cluster was prepared by the reductive decomposition of Ag(I)SG thiolate in gel cavities following a method previously reported from our lab³¹ (Scheme 1). In brief, a mixture of AgNO_3 and GSH was (in 1:2 molar ratio) dissolved in NaOH solution (45 mg NaOH in 1 mL distilled water) at room temperature and sonicated for a few minutes. A yellow solution of Ag(I)SG complexes was obtained. It was added to 4.2 mL of gel (44 g of acrylamide and 3 g of BIS mixed with 100 mL of distilled water). To this mixture, 50 μL of 0.1% solution of ammonium persulfate and 40 μL of TEMED were added, which resulted in the formation of a gel. The gel was kept undisturbed for 20 min at room temperature and then at ice cold temperature for 10 min. A solution of 100 mg NaBH_4 in 10 mL of ice-cold water was added to the gel and kept undisturbed at 0 °C for about 0.5 h. The color of the gel changed from yellow to brown, indicating the formation of clusters within the gel. The dark-brown-colored gel was transferred to a mortar, crushed, and washed many times with methanol to remove excess NaBH_4 . The crushed gel was taken, and distilled water was added to extract the cluster into the aqueous medium. The yield of the cluster was 66% with respect to AgNO_3 .

2.3. Thermal Decomposition of the Clusters. The cluster solution was kept in a synthesizer under constant stirring at 80 °C until the color changed from reddish brown to greenish black, which took about 30 h. After cooling, it was centrifuged to get a greenish black residue. The clear supernatant solution was preserved for further characterizations.

2.4. Characterization. Optical absorption spectra were collected in the range 200 to 1100 nm. For room-temperature recordings, a Perkin-Elmer Lambda-25 spectrophotometer was used. For higher temperature recordings, another Perkin-Elmer spectrometer, with an accessory for maintaining sample temperature, was used. Luminescence spectra were recorded using a Jobin Yvon Nano Log spectrofluorimeter. Scanning electron microscopic (SEM) images and EDAX images were obtained using a FEI QUANTA-200 SEM. For measurements, samples were prepared by drop casting on an indium tin oxide (ITO)-coated glass plate and drying in vacuum. The X-ray diffractogram was collected using $\text{Cu K}\alpha$ radiation ($\lambda = 1.5418 \text{ \AA}$) in a Bruker AXS D8 Discover diffractometer. Transmission electron microscopy (TEM) measurements were carried out using a JEOL 3011 instrument. Samples for TEM were prepared by dropping the aqueous dispersions on amorphous carbon films supported on a copper grid and drying in an ambient atmosphere. Mass spectra were recorded using a QTrap 3200 instrument with electrospray ionization (ESI). Samples of 20 ppm concentration (in Ag), prepared using 1:1 mixture of CH_2Cl_2 /methanol, were electrosprayed at a flow rate of 10 $\mu\text{L}/\text{min}$ and at an ion spray voltage of 5 kV.

2.5. Results and Discussion. The absorption spectrum of freshly prepared clusters in aqueous medium (Figure S1 of the Supporting Information) confirms the formation of $\text{Ag}_{25}\text{SG}_{18}$ clusters.³¹ Unlike larger Ag nanoparticles, which show surface plasmon resonance (SPR) at $\sim 400 \text{ nm}$, Ag_{25} clusters show molecule-like transitions, as revealed in their absorption spectrum, having (i) a pronounced peak at 478 nm and (ii) two broad peaks at 330 and 640 nm. The molecular-like energy levels are mostly derived from sp orbitals of silver.¹² The optical absorption spectrum of the freeze-dried cluster sample was also taken after redispersing the dried powder in water. The features at 330, 478, and 640 nm in the UV/vis spectrum of the redispersed sample indicate the presence of the cluster (Figure S2 of the Supporting Information). The inset in Figure S1 of the Supporting Information shows the TEM image of clusters. No individual cluster is seen in the image because the core dimension is small ($< 1 \text{ nm}$). Also, such clusters are highly sensitive to electron beam

in TEM; they aggregate to form nanoparticles instantaneously upon electron beam irradiation.^{32,33}

Time-dependent absorption spectra of $\text{Ag}_{25}\text{SG}_{18}$ cluster were taken at room temperature, which show a gradual decrease in the intensities of the peaks at 330, 478, and 640 nm with time (Figure S3 of the Supporting Information). The peaks at 330 and 640 nm are more sensitive and vanish at a faster rate compared with the prominent peak at 478 nm, which shows reasonable peak intensity even after 90 days. This type of behavior in the absorption spectra is observed for previously reported thiolate-protected silver clusters.³⁴ The thermal stability of these clusters was examined by taking UV/vis spectra at several fixed temperatures in the range of 25–85 °C (Figure 1). We see that the peak position

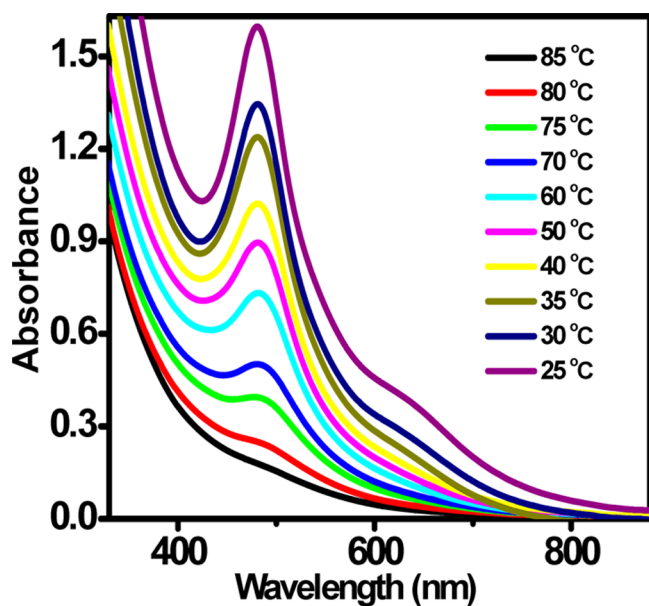


Figure 1. UV/vis spectra of $\text{Ag}_{25}\text{SG}_{18}$ clusters at various temperatures ranging from 25 to 85 °C.

remains the same, whereas peak intensities decrease with increase in temperature. Similar to the behavior in the time-dependent spectra, the peaks at 330 and 640 nm vanish very fast compared with the peak at 478 nm. Although there is a decrease in intensity with temperature, clusters seem to be almost stable up to 50 °C, as revealed by the persistence of the peak at 478 nm. Above 50 °C,

even the peak at 478 nm decreases at a faster rate, finally showing a featureless spectrum. The decomposition follows first-order kinetics, as revealed by analysis of absorption spectra, shown in Figure S4 of the Supporting Information. One of the products of decomposition is silver sulphide, the presence of which is confirmed by EDAX and XRD. (See Figures 3 and 4.)

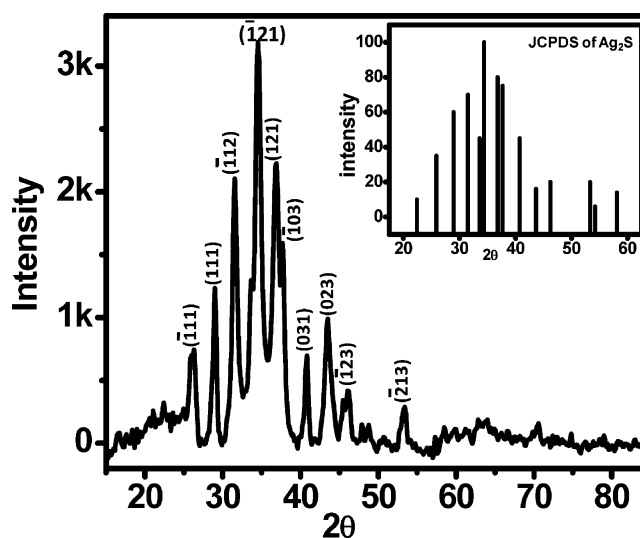


Figure 3. X-ray diffraction pattern of residue obtained after decomposition of $\text{Ag}_{25}\text{SG}_{18}$ clusters. Inset shows the standard pattern of monoclinic form of Ag_2S .

For obtaining the decomposed end product for further characterization, an aqueous solution of clusters was heated to 80 °C for 30 h with constant stirring. The resulting mixture was freeze-dried to get a greenish black solid residue. Figure 2A shows the absorption spectrum of this residue after suspending in water. We see that the peaks, characteristic of clusters, have vanished, and very broad and shallow features are observed. Starting from the beginning of heating at 80 °C, the color of the solution changed from brownish red to a reddish orange and then finally to greenish black, as shown in the photograph (Figure 2A (a–c)). The inset of Figure 2A shows the Jacobian-corrected spectrum of the greenish black residue, where absorption features at ~340 and ~770 nm are seen. To amplify less-intense absorption features, we have corrected the data with the Jacobian factor. For this, the experimentally obtained intensities in absorbance as a

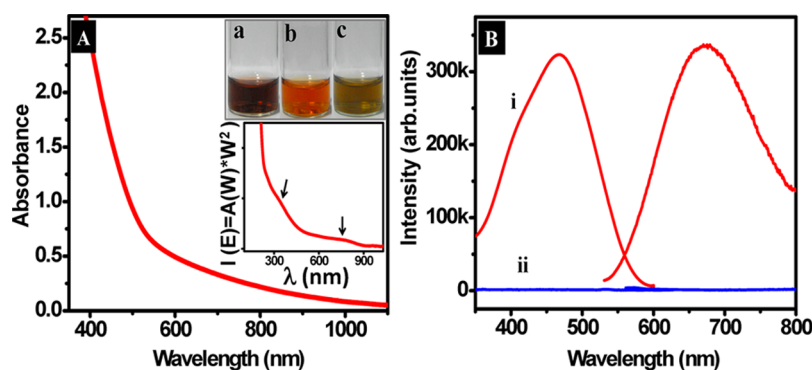


Figure 2. (A) UV/vis spectrum of product (Ag_2S) obtained by complete decomposition of $\text{Ag}_{25}\text{SG}_{18}$ clusters. The bottom inset of panel A shows the Jacobian corrected spectrum. The upper inset gives the photographs of clusters in various stages during thermal decomposition. (a) As-synthesized clusters in water. (b) After 20 h of heating at 80 °C. (c) After heating for 30 h at 80 °C. (B) Excitation and emission spectra of $\text{Ag}_{25}\text{SG}_{18}$ (i, red trace) and that of the decomposed sample in water at 25 °C (ii, blue trace).

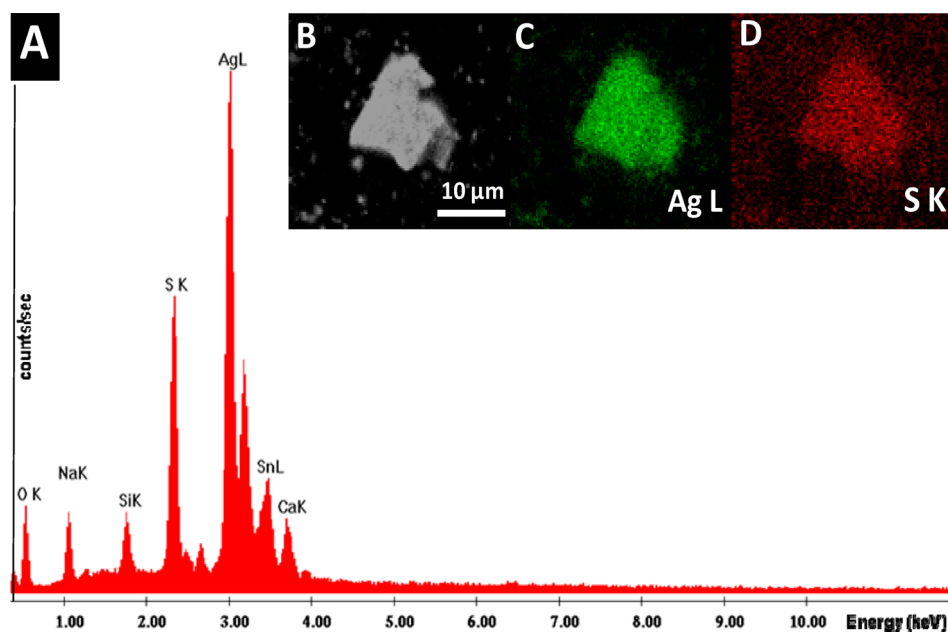


Figure 4. (A) EDAX spectrum of the residue left after decomposition of $\text{Ag}_{25}\text{SG}_{18}$ clusters. (B) Its SEM image and EDAX images collected using Ag $L\alpha$ (C) and S $K\alpha$ (D).

function of wavelength $[I(W)]$ have been converted to energy-dependent values $[I(E)]$ using the expression $I(E) = I(W)/(\partial E/\partial W) \propto I(W) \cdot W^2$, where $\partial E/\partial W$ represents the Jacobian factor against wavelength. The onset of absorption is observed at ~ 950 nm. All of these are attributed to band-edge transitions in silver sulphide nanoparticles. Similar absorption band positions and band profile are seen in the UV/vis spectrum of Ag_2S nanocrystals.^{35–37,39} The luminescence profile of the as-prepared clusters and of the decomposed sample are shown in Figure 2B. Ag_{25} clusters exhibit a red emission peaking at 650 nm when excited with 480 nm radiation. In contrast, the decomposed sample did not show luminescence for the same excitation.

Direct confirmation of the formation of Ag_2S nanoparticles is obtained from the XRD pattern (Figure 3) of the solid product. The pattern shows prominent peaks corresponding to diffraction from (111), (−111), (112), (121), (−103), (−023), (−123), and (−213) crystal planes of room temperature modification (Acanthite, monoclinic) of Ag_2S ³⁸ (JCPDS file no: 14-0072, inset of Figure 3.). Acanthite is stable at temperatures < 176 °C.^{39,40} The other phases of Ag_2S , such as body-centered cubic (argentite) and face-centered cubic (high argentite) forms, exist at high temperatures. These phases are not present in the present system. The absence of silver nanoparticles and silver thiolate is confirmed by XRD as well. This XRD taken for the decomposed sample is different from that of the parent $\text{Ag}_{25}\text{SG}_{18}$ cluster, which shows a broad peak at 36° (2θ) (Figure S5 of the Supporting Information). Slightly broader peaks observed in our diffraction pattern of the decomposed sample as compared with that of well-crystallized samples are ascribed to the smaller grain size of the former.

EDAX of the final solid (Figure 4A) shows the atomic ratio of Ag:S in the final product to be 2:1, as expected for stoichiometric Ag_2S . Figure 4B gives the SEM image of the product. Figure 4C,D is the EDAX image collected using Ag $L\alpha$ and S $K\alpha$, respectively. Peaks of other elements such as O, Si, Sn, and Ca are also present in the EDAX spectrum, which are due to elements present in the ITO-coated glass plate.

The shape and distribution of Ag_2S nanoparticles were studied by TEM (Figure 5). Monodispersed spherical nanoparticles with

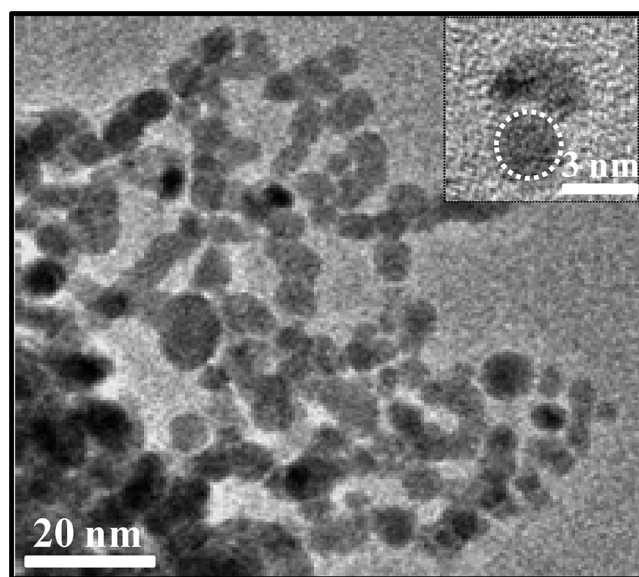


Figure 5. TEM image of the decomposed sample showing nanoparticles. Inset shows the image of a single nanoparticle at a higher magnification.

a mean diameter of 3 ± 1 nm are seen in the images. Aggregation is expected because of the lack of surface protection. The large number of aggregates seen in the image is due to high particle concentration in the solution used for analysis. The Ag_2S nanoparticles formed in the present study are very small in size in comparison with that of Ag_2S nanoparticles synthesized by previously reported methods, employing other wet chemical routes, the minimum mean diameter reported being ~ 8 nm. Although XRD revealed the presence of distinct lattice planes, TEM images did not show them because particles are very small.

Thermal decomposition of $\text{Ag}_{25}\text{SG}_{18}$ clusters at comparatively high temperatures (~ 80 °C) for long time seems to favor the breaking of sulfur–carbon bond (S–C bond) of the thiol ligand rather than the silver–sulfur bond (Ag–S bond). The organic

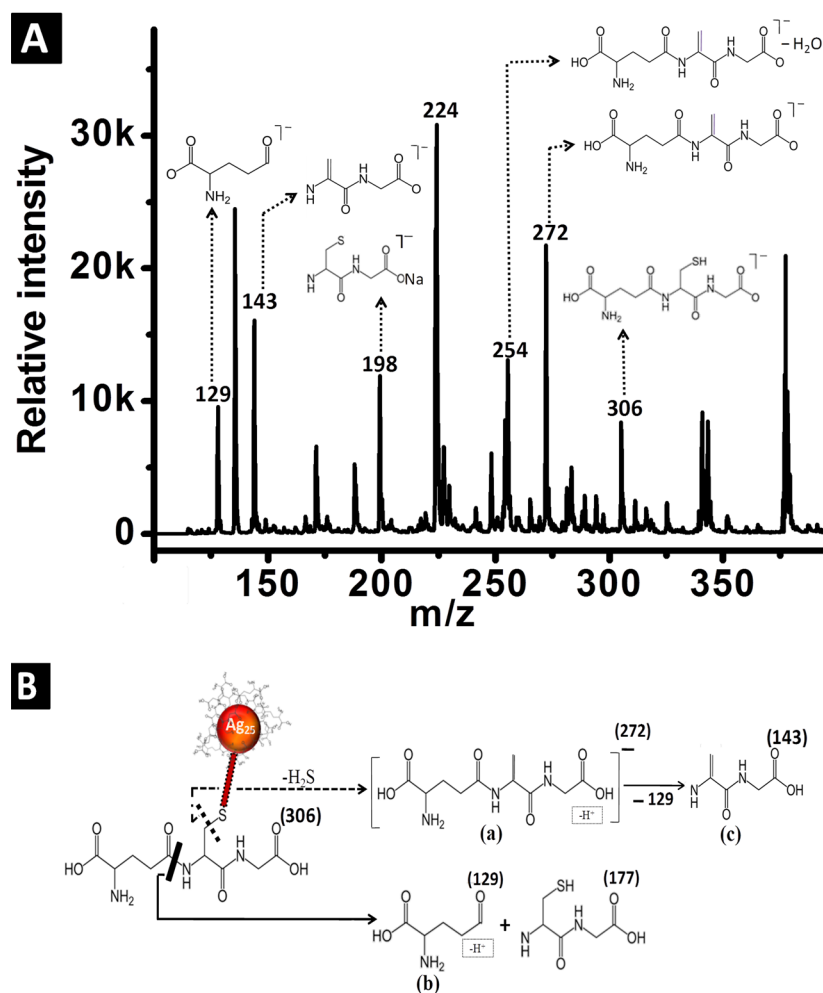


Figure 6. (A) Portion of negative ion ESI MS of the supernatant solution left after the removal of solid products obtained after decomposition of $\text{Ag}_{25}\text{SG}_{18}$. (B) Scheme showing the possible fragmentation path for glutathione molecules bonded to the Ag core.

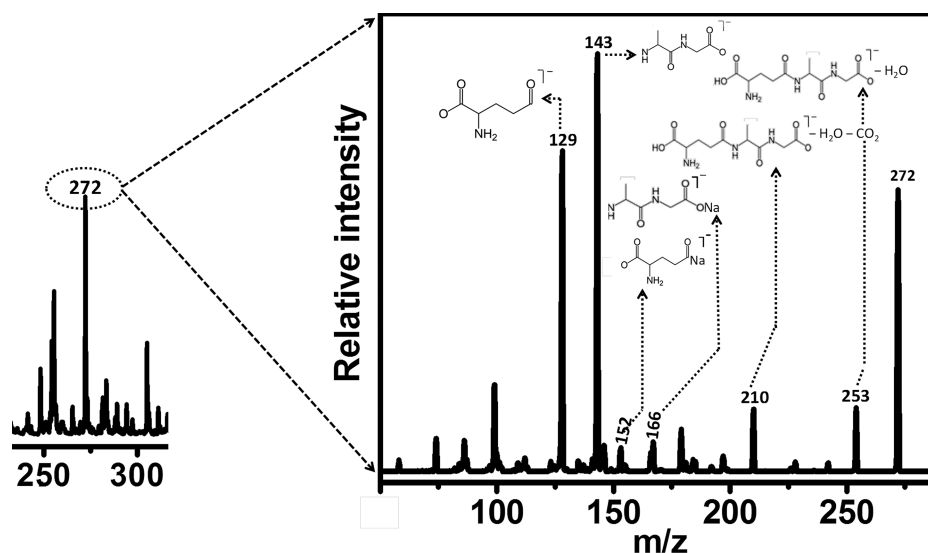
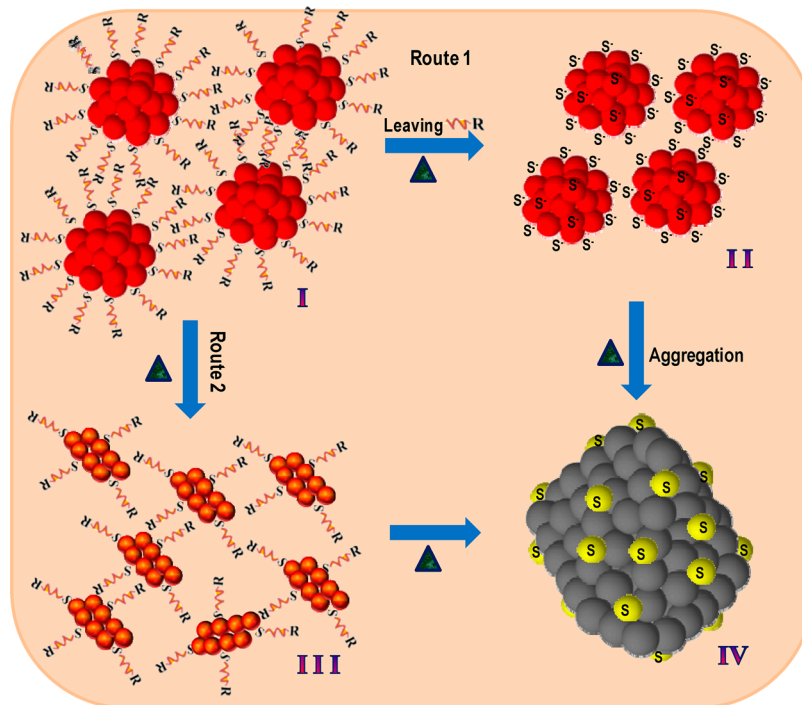


Figure 7. MS/MS of desulphurized glutathione peak at m/z 272. Spectrum on the left shows the peak selected for MS/MS analysis.

moieties formed after dissociation go to the solution, leaving stable Ag_2S . The presence of desulphurized organic entities of GSH was confirmed by ESI MS of the supernatant solution left after the removal of the solid product (Figure 6A). Only the significant portion of the mass spectrum is shown in Figure 6A.

Schematics shown in Figure 6B give the possible bond cleavage schemes of GSH upon temperature-induced decomposition application. The fragmentation results in two kinds of products: (i) a desulphurized GSH (as in scheme (a)) and (ii) two asymmetric fragments of SGH (as in schemes (b) and (c)). Mass

Scheme 2. Schematic Representation of Two Possible Routes for the Formation of Ag₂S Nanoparticles from Ag₂₅SG₁₈ Clusters^a

^a(I) Parent Ag₂₅SG₁₈ cluster before heating, (II) Ag–S moiety formed due to heating, (III) Ag(I)-thiolates formed upon heating, and (IV) the final product obtained after decomposition (Ag₂S NPs).

spectrum, taken in the negative mode, shows a peak at m/z 272, which we assign to desulphurized species. The peak at m/z 306 is assigned to reduced GSH. We can also see a number of small fragments of GSH in the mass spectrum. The formation of some prominent fragments is explained through the scheme presented in Figure 6B. Peaks appear at the calculated positions for GSH.⁴¹ For example, the peak due to the first fragment (in scheme (b)) is at m/z 129, and that at m/z 143 (in scheme (c)) can be attributed to the removal of neutral pyroglutamic acid from desulphurized species. A peak at m/z 198 (Figure 6A) is due to the presence of the second fragment in which proton is replaced by a Na⁺, that is present in the medium. The peak at m/z 254 is due to the species formed by the loss of one water molecule from the desulphurized GSH species. Along with these peaks, there are some peaks originating from a small amount of acrylamide gel still remaining in solution (for example, the peak at m/z 224). The mass spectrum in the positive ion mode also shows all of these peaks (not shown here). The mass spectrum collected for GSH alone, in the negative mode, also shows similar peaks at corresponding m/z values (Figure S6 of the Supporting Information), which further justifies our result.

Figure 7 shows the MS/MS spectrum of the peak at m/z 272. MS/MS gives major fragment peaks at m/z 129, 143, 210, and 253. The formation of these fragments is explained in Figure 6. Peaks at m/z 152 and 165 are assigned, respectively, to species formed by the replacement of protons in fragments, m/z 129 and 143 by Na⁺.

The mechanism of formation of silver sulphide nanoparticles is not well understood. Here we present our tentative suggestions for the formation of Ag₂S upon thermal decomposition of silver quantum clusters.

There are two possible routes for the dissociation of thiolates on cluster surfaces, as shown in Scheme 2. In the first case, the organic moiety, devoid of sulfur, leaves the cluster surface, resulting

in silver sulphide nuclei of the form Ag₂₅S₁₂; subsequently, these aggregate to form Ag₂S nanoparticles (Route 1). Assuming the structure of Ag₂₅SG₁₈ to be similar to that of Au analogue, there could be SG ligands directly bonded to the core along with bridged ligands. Probably, it is these bridged species that are thermally less stable,⁴³ and they get desorbed with activation. This desorption could explain the presence of anionic GSH seen in the mass spectrum of the solution. MALDI mass spectra of such clusters, where Au₂₅SR₁₂ fragments were observed, also support this view.^{42,43} Analogous entities existing in solution might have undergone thermal cleavage, leading to Ag₂₅S₁₂. We note that the Ag to S ratio, 25:12, is very close to the ideal ratio, 25:12.5, needed for the formation of stoichiometric Ag₂S. The extent of nonstoichiometry due to lower sulfur content, if it exists, would be very small. The organic moieties go to the supernatant solution as previously described. In the second case, Ag(I) thiolates are formed by thermal decomposition of the cluster and eventually Ag₂S nanoparticles formed by continuous heating (Route 2). Route 2 may be better feasible thermodynamically because the formation of thiolates is commonly seen from such clusters. Thiolates, once formed, can have two possible cleavages, namely, at the Ag–S bond (eq 1) and at the C–S bond (eq 2).



The changes in enthalpy of formation for the two reactions were calculated.

$$\Delta H_1 = \Delta_f H^\circ(\text{R-S-S-R}) + \Delta_f H^\circ(\text{Ag}) - 2\Delta_f H^\circ(\text{R-S-Ag}) \quad (1a)$$

$$\Delta H_2 = \Delta_f H^\circ(\text{R-S-R}) + \Delta_f H^\circ(\text{Ag}_2\text{S}) - 2\Delta_f H^\circ(\text{R-S-Ag}) \quad (2a)$$

These prototypical reactions represent the formation of silver nanoparticles or Ag_2S nanoparticles. The enthalpy of formation of Ag_2S is -32.6 kJ/mol. The possible entities upon heating, R-S-R and R-S-S-R, were taken to be dimethyl sulphide and dimethyl disulfide, respectively, and the corresponding values of enthalpy of formation of are -65.3 and -62.6 kJ/mol.⁴⁴ Absolute values of ΔH_1 and ΔH_2 could not be calculated because the heat of formation of R-S-Ag is not available. However, it can be seen that ΔH_2 is more negative than ΔH_1 , and hence the formation of Ag_2S is more feasible than that of Ag nanoparticles.

From the above discussion, it is clear that Ag_2S can be formed either through direct dissociation or through the thiolate intermediate. In the first, thermodynamic values of the corresponding model systems are not available to evaluate the enthalpies. In the second case, a preliminary thermodynamic evaluation supports the experimental observation.

The presence of Ag^+ and Ag nanoparticles in the mother liquor was also evaluated. Typically the presence of Ag^+ is assessed using the precipitation of AgCl upon the addition of NaCl , and that of Ag nanoparticles is assessed using their characteristic optical absorption, which is dominated by SPR at 400 nm. We did not observe any ionic Ag species in solution, nor did we have nanoparticles of silver.

3. CONCLUSIONS

In summary, temperature-dependent studies were performed on silver quantum clusters, which exhibit distinct nonplasmonic features in their absorption spectrum. Results presented here suggest that thermal decomposition of these quantum clusters follows a mechanism that is significantly different from that of their larger analogues, namely, nanoparticles. Whereas the direct desorption of disulfide, resulting in the formation of bulk silver, is seen in the case of nanoparticles, C–S bond cleavage occurs in quantum clusters, resulting in the formation of silver sulphide nanoparticles. The difference in ligand binding strength is manifested in the observed product. We have used spectroscopic studies to understand an approximate chemical reaction for the process. An extension of the study to diverse quantum clusters in different media may lead to new products of different morphologies.

■ ASSOCIATED CONTENT

● Supporting Information

Preliminary confirmation of cluster formation through UV/vis profile and a TEM image, time-dependent UV/vis spectra of $\text{Ag}_{25}\text{SG}_{18}$ quantum cluster, and kinetics of decomposition. This material is available free of charge via the Internet at <http://pubs.acs.org>.

■ AUTHOR INFORMATION

Corresponding Author

*Phone: +91-44-2257 4208. Fax: +91-44-2257 0509/0545. E-mail: pradeep@iitm.ac.in.

Notes

The authors declare no competing financial interest.

■ ACKNOWLEDGMENTS

We thank the Department of Science and Technology (DST), Government of India, for constantly supporting our research program on nanomaterials.

■ REFERENCES

- (1) Brust, M.; Walker, M.; Bethell, D.; Schiffrin, D. J.; Whyman, R. J. *Chem. Soc., Chem. Commun.* **1994**, 801–802.
- (2) Templeton, A. C.; Wuelfing, W. P.; Murray, R. W. *Acc. Chem. Res.* **2000**, *33*, 27–36.
- (3) Sandhyarani, N.; Pradeep, T. *Int. Rev. Phys. Chem.* **2003**, *22*, 221–262.
- (4) (a) Daniel, M.-C.; Astruc, D. *Chem. Rev.* **2004**, *104*, 293–346. (b) Brust, M.; Kiely, C. J. In *Colloids and Colloid Assemblies: Synthesis, Modification, and Utilization of Colloid Particles*; Wiley: Weinheim, Germany, 2004; pp 96–119.
- (5) (a) Delemarche, E.; Michel, B.; Kang, H.; Gerber, C. *Langmuir* **1994**, *10*, 4103–4108. (b) Schreiber, F. *Prog. Surf. Sci.* **2000**, *65*, 151–256. (c) Terrill, R. H.; Postlethwaite, T. A.; Chen, C.-H.; Poon, C.-D.; Terzis, A.; Chen, A.; Hutchison, J. E.; Clark, M. R.; Wignall, G.; Londono, J. D.; Superfine, R.; Falvo, M.; Johnson, C. S.; Samulski, E. D.; Murray, R. W. *J. Am. Chem. Soc.* **1995**, *117*, 12537–12548.
- (6) Nuzzo, R. G.; Korenic, E. M.; Dubois, L. H. *J. Chem. Phys.* **1990**, *93*, 767–773.
- (7) Murty, K. V. G. K.; Venkataraman, M.; Pradeep, T. *Langmuir* **1998**, *14*, 5446–5456.
- (8) Buttner, M.; Belser, T.; Oelhafen, P. *J. Phys. Chem. B* **2005**, *109*, 5464–5467.
- (9) (a) Fields, E. K.; Meyerson, S. J. *Org. Chem.* **1976**, *41*, 916–920. (b) Lee, S. J.; Han, S. W.; Choi, H. J.; Kim, K. J. *Phys. Chem. B* **2002**, *106*, 2892–2900. (c) Choi, H. J.; Han, S. W.; Lee, S. J.; Kim, K. J. *Colloid Interface Sci.* **2003**, *264*, 458–466.
- (10) (a) Pradeep, T.; Sandhyarani, N. *Pure Appl. Chem.* **2002**, *74*, 1593–1607.
- (11) (a) Devadas, M. S.; Bairu, S.; Qian, H.; Sinn, E.; Jin, R.; Ramakrishna, G. *J. Phys. Chem. Lett.* **2011**, *2*, 2752–2758. (b) Kumar, S.; Jin, R. *Nanoscale* **2012**, *4*, 4222–4227.
- (12) Bakr, O. M.; Amendola, V.; Aikens, C. M.; Wenseleers, W.; Li, R.; Negro, L. D.; Schatz, G. C.; Stellacci, F. *Angew. Chem., Int. Ed.* **2009**, *48*, 5921–5926.
- (13) (a) Branham, M. R.; Douglas, A. D.; Mills, A. J.; Tracy, J. B.; White, P. S.; Murray, R. W. *Langmuir* **2006**, *22*, 11376–11383. (b) Zheng, J.; Petty, J. T.; Dickson, R. M. *J. Am. Chem. Soc.* **2003**, *125*, 7780–7781. (c) Rao, T. U. B.; Nataraju, B.; Pradeep, T. *J. Am. Chem. Soc.* **2010**, *132*, 16304–16307. (d) Jin, R. *Nanoscale* **2010**, *2*, 343–362.
- (14) Muhammed, M. A. H.; Pradeep, T. In *Advanced Fluorescence Reporters in Chemistry and Biology II*; Demchenko, A. P., Ed.; Springer-Verlag: Berlin, 2010; Vol. 9, p 333 and references cited therein.
- (15) Muhammed, M. A. H.; Ramesh, S.; Sinha, S. S.; Pal, S. S.; Pradeep, T. *Nano Res.* **2008**, *1*, 333–340.
- (16) Diez, I.; Ras, R. H. A. *Nanoscale* **2011**, *3*, 1963–1970.
- (17) Toikkanen, O.; Carlsson, S.; Dass, A.; Rönholm, G.; Kalkkinen, N.; Quinn, M. B. *J. Phys. Chem. Lett.* **2010**, *1*, 32–37.
- (18) Lourdu Xavier, P.; Chaudhari, K.; Bakshi, A.; Pradeep, T. *Nano Res.* **2012**, *3*, 14767.
- (19) Triulzi, R. C.; Micic, M.; Giordani, S.; Serry, M.; Chiou, W. A.; Leblanc, R. M. *Chem. Commun.* **2006**, *48*, 5068–5070.
- (20) Wu, X.; He, X.; Wang, K.; Xie, C.; Zhou, B.; Qing, Z. *Nanoscale* **2010**, *2*, 2244–2249.
- (21) Zhang, X.-D.; Wu, D.; Shen, X.; Liu, P.-X.; Fan, F.-Y.; Fan, S.-J. *Biomaterials* **2012**, *33*, 4628–4638.
- (22) Shibu, E. S.; Radha, B.; Verma, P. K.; Bhyrappa, P.; Kulkarni, G. U.; Pal, S. K.; Pradeep, T. *ACS Appl. Mater. Interfaces* **2009**, *1*, 2199–2210.
- (23) Lewis, L. N. *Chem. Rev.* **1993**, *93*, 2693–2730.
- (24) Sanchez, A.; Abbet, S.; Heiz, U.; Schneider, W. D.; Häkkinen, H.; Barnett, R. N.; Landman, U. *J. Phys. Chem. A* **1999**, *103*, 9573–9578.
- (25) Zhu, Y.; Qian, H.; Drake, B. A.; Jin, R. *Angew. Chem., Int. Ed.* **2010**, *49*, 1295–1298. Leelavathi, A.; Rao, T. U. B.; Pradeep, T. *Int. J. Nanosci.* **2011**, *10*, 839–843.
- (26) Muhammed, M. A. H.; Pradeep, T. *Chem. Phys. Lett.* **2007**, *449*, 186–190.

- (27) (a) Bootharaju, M. S.; Pradeep, T. *Langmuir* **2011**, *27*, 8134–8143. (b) Liu, H.; Zhang, X.; Wu, L.; Jiang, L.; Burda, C.; Zhu, J. *Chem. Commun.* **2011**, *47*, 4237–4239.
- (28) (a) Adhikari, B.; Banerjee, A. *Chem. Mater.* **2010**, *22*, 4364–4371. (b) Liu, S.; Lu, F.; Zhu, J.-J. *Chem. Commun.* **2011**, *47*, 2661–2663.
- (29) (a) Muhammed, M. A. H.; Verma, P. K.; Pal, S. K.; ArunKumar, R. C.; Paul, S.; OmKumar, R. V.; Pradeep, T. *Chem.—Eur. J.* **2009**, *15*, 10110–10120. (b) Yu, J.; Choi, S.; Dickson, R. M. *Angew. Chem., Int. Ed.* **2009**, *48*, 318–320.
- (30) Verma, A.; Uzun, O.; Hu, Y. H.; Hu, Y.; Han, H. S.; Watson, N.; Chen, S. L.; Irvine, D. J.; Stellacci, F. *Nat. Mater.* **2008**, *7*, 588.
- (31) (a) Cathcart, N.; Kitaev, V. *J. Phys. Chem. C* **2010**, *114*, 16010–16017. (b) Chakraborty, I.; Udayabhaskararao, T.; Pradeep, T. *J. Hazard. Mater.* **2012**, *211–212*, 396–403.
- (32) Shibu, E. S.; Habeeb Muhammed, M. A.; Tsukuda, T.; Pradeep, T. *J. Phys. Chem. C* **2008**, *112*, 12168–12176.
- (33) Rao, T. U. B.; Pradeep, T. *Angew. Chem., Int. Ed.* **2010**, *49*, 3925–3929.
- (34) Cathcart, N.; Mistry, P.; Makra, C.; Pietrobon, B.; Coombs, N.; Niaraki, M. J.; Kitaev, V. *Langmuir* **2009**, *25*, 5840–5846.
- (35) Pileni, M. P.; Motte, L.; Billoudeet, F.; Mahrt, J.; Willig, F. *Mater. Lett.* **1997**, *31*, 255–260.
- (36) Leon-Velazquez, M. S.; Irizarry, R.; Castro-Rosario, M. E. *J. Phys. Chem. C* **2010**, *114*, 5839–5849.
- (37) Chen, R.; Nuhfer, N. T.; Moussa, L.; Morris, H. R.; Whitmore, P. M. *Nanotechnology* **2008**, *19*, 455604–455615.
- (38) Karimzadeh, R.; Aleali, H.; Mansour, N. *Opt. Commun.* **2011**, *284*, 2370–2375.
- (39) Aleali, H.; Sarkhosh, L.; Karimzadeh, R.; Mansour, N. *Phys. Status Solidi B* **2011**, *248*, 680–685.
- (40) Martinez-Castañón, G. A.; Sánchez-Loredo, M. G.; Dorantes, H. J.; Martinez-Mendoza, J. R.; Ortega-Zarzosa, G.; Ruiz, F. *Mater. Lett.* **2005**, *59*, 529–534.
- (41) Thakur, S. S.; Balaram, P. *J. Am. Soc. Mass. Spectrom.* **2008**, *19*, 358–366.
- (42) Wu, Z.; Gayathri, C.; Gil, R. R.; Jin, R. *J. Am. Chem. Soc.* **2009**, *131*, 6535–6542.
- (43) Wu, Z.; Jin, R. *ACS Nano* **2009**, *3*, 2036–2042.
- (44) Lide, D. R. *Handbook of Chemistry and Physics*, 80th ed.; CRC Press: Boca Raton, FL, 1999–2000; pp 5–31.